The Zinc Finger of NEMO Is a Functional Ubiquitin-binding Domain*[S]

Florence Cordier[‡1,2], Olivera Grubisha[§1,3], François Traincard[§], Michel Véron[§], Muriel Delepierre[‡], and Fabrice Agou[§4]

From the Institut Pasteur, ‡Unité de Résonance Magnétique Nucléaire des Biomolécules and §Unité de Biochimie Structurale et Cellulaire, CNRS, URA 2185, 25/28 rue du Dr. Roux, F-75015 Paris, France

NEMO (NF-κB essential modulator) is a regulatory protein essential to the canonical NF-κB signaling pathway, notably involved in immune and inflammatory responses, apoptosis, and oncogenesis. Here, we report that the zinc finger (ZF) motif, located in the regulatory C-terminal half of NEMO, forms a specific complex with ubiquitin. We have investigated the NEMO ZF-ubiquitin interaction and proposed a structural model of the complex based on NMR, fluorescence, and mutagenesis data and on the sequence homology with the polymerase η ubiquitin-binding zinc finger involved in DNA repair. Functional complementation assays and in vivo pull-down experiments further show that ZF residues involved in ubiquitin binding are functionally important and required for NF-κB signaling in response to tumor necrosis factor-α. Thus, our findings indicate that NEMO ZF is a bona fide ubiquitin-binding domain of the ubiquitin-binding zinc finger type.

The NF-κB transcription factors regulate the expression of genes involved in inflammation, immunity, cell proliferation, apoptosis, and oncogenesis (1). The classical NF-κB signaling pathway is induced in response to proinflammatory cytokines (interleukin-1, TNF-α),[5] antigens, and endotoxins. Although different receptors and downstream molecules are engaged depending on the stimulus, they all transduce signals through the IKK complex. These active complexes comprise two catalytic kinase subunits, IKKα and/or IKKβ, and a dimer of regulatory subunits termed NEMO, which is required for IKK complex activity and subsequent NF-κB activation (2, 3).

The N-terminal part of NEMO interacts with the IKK kinases, whereas the regulatory C-terminal half is involved in signal recognition (4, 5). The latter comprises the CC2-LZ domain, including a coiled-coil (CC2) and a leucine zipper (LZ) motif and a CCHC-type zinc finger (ZF) domain (Fig. 1). The CC2-LZ domain is required for NEMO oligomerization (6, 7) and contains a ubiquitin-binding domain (UBD) that preferentially interacts with Lys-63-polyubiquitin (Lys-63-polyUb) chains (8, 9). Lys-63-polyUb binding through the CC2-LZ domain of NEMO is required for NF-κB signaling from several different receptors. In the case of TNF-α receptor 1 (TNFR1), the IKK complex seems to be recruited to the TNFR1 receptor via interaction with Lys-63-polyubiquitinated RIP1 protein (8, 9). In addition to binding Lys-63-polyUb, a minor fraction of NEMO undergoes ubiquitination (post-translational modification via the covalent attachment of ubiquitin) within the regulatory portion of NEMO. Several monoubiquitination and Lys-63-polyubiquitination sites on NEMO have been identified, including a Lys-399 residue in the ZF domain (10), and the site of modification and its impact on IKK activity appear to be signal-dependent (11–13).

Although the CC2-LZ domain of NEMO is required for a wide range of NF-κB-inducing signals, the role of the NEMO ZF domain remains controversial (14, 15) and appears to depend on the stimulus. Several studies reported that NEMO ZF is required for interleukin-1 and TNF-α but not lipopolysaccharide-induced signaling (16, 17). On the other hand, a clear requirement for ZF in the genotoxic stress response has been established (12, 18). This distinct pathway is activated by UV radiation and other DNA-damaging agents and involves import of NEMO into the nucleus, where it interacts with the ataxia telangiectasia mutated (ATM) checkpoint kinase. The importance of NEMO ZF is also emphasized by the fact that (i) several mutations in the ZF are linked to the human diseases, anhidrotic ectodermal dysplasia with immunodeficiency and incontinentia pigmenti (19), and that (ii) mice lacking the NEMO ZF die during embryonic development (20).

We recently determined the solution structure of NEMO ZF (21), which highlighted the importance of a large hydrophobic cluster sharing similarities with the ubiquitin-interacting region of the ubiquitin-binding ZF (UBZ) of the human DNA Y-polymerase (pol) η (22). Because UBDs are usually found in multiple copies in proteins, the question arises whether NEMO ZF could actually act as a second ubiquitin-binding site, in addition to the CC2-LZ domain. We show here, using NMR, fluorescence, mutagenesis, and in vivo pull-down experiments, that NEMO ZF is a bona fide UBD of the UBZ type. We have investigated the ZF-ubiquitin interaction, proposed a model of the

[1] Both authors contributed equally to this work.

[2] To whom correspondence may be addressed. Tel.: 33-1-45-68-88-73; Fax: 33-1-45-68-89-29; E-mail: fcordier@pasteur.fr.

[3] Recipient of a Pasteur Foundation fellowship.

[4] To whom correspondence may be addressed. Tel.: 33-1-44-38-95-69; Fax: 33-1-45-68-83-99; E-mail: fagou@pasteur.fr.

[5] The abbreviations used are: TNF-α, tumor necrosis factor α; IKK, IκB kinase; WT, wild type; NEMO, NF-κB essential modulator; ZF, zinc finger; LZ, leucine zipper; UBZ, ubiquitin-binding ZF; UBD, ubiquitin-binding domain; UIM, ubiquitin-interacting motif; polyUb, polyubiquitin; pol, polymerase; NOE, nuclear Overhauser effect; CC, coiled-coil.
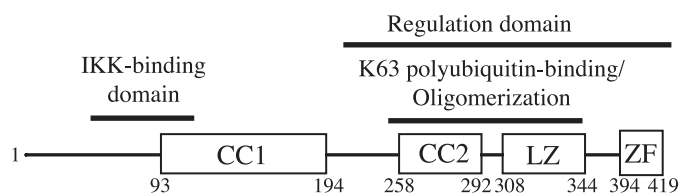
FIGURE 1. **Structural and functional domains of the NEMO protein.** Structural domains include the coiled-coil (CC1 and CC2), LZ, and ZF motifs. The functional NEMO domains are indicated on the *top*. Sequence numbering is given for the human NEMO protein.

complex, and further showed that ZF residues involved in ubiquitin binding are functionally important and required for NF-κB signaling in response to TNF-α.

EXPERIMENTAL PROCEDURES

Sample Preparation—NEMO ZF synthetic peptides (>98% purity) termini-blocked by *N*-acetyl and C-amide groups were purchased from Biopeptide Co. (San Diego, CA). Five different peptides were used in this study; ZF corresponds to 2 Ser residues followed by residues 394–419 of human NEMO. In ZF(W), Phe-395 is replaced by a tryptophan. ZF(W)-M407V, ZF(W)-V414S, and ZF(W)-M415S are three point mutant peptides of ZF(W). The sequences are given in supplemental Fig. S1. For binding assays, each of the four ZF(W) peptides was solubilized in a buffer of 0.6 mM $ZnCl_2$, 1 mM tris(2-carboxyethyl)phosphine, and 50 mM Tris-HCl (pH 7.5) to a stock concentration of ~0.2 mM. Recombinant human ubiquitin and the I44A ubiquitin mutant were purchased from Boston Biochem at >95% purity. Ubiquitin was further purified by cation exchange column, dialyzed in water, lyophilized, and solubilized in 50 mM Tris-HCl (pH 7.5). For NMR, 1.7 mM of the ZF was prepared by dissolving 2.8 mg of peptide in 500 μl of 3.4 mM $ZnCl_2$, 3.4 mM tris(2-carboxyethyl)phosphine, 20 mM Tris-HCl, 90% H_2O, 10% D_2O (pH 6.2). The U-^{15}N-labeled human ubiquitin was purchased from VLI Research Inc. (Malvern, PA), and a 1 mM stock solution was prepared in exactly the same buffer as the ZF. Three NMR samples of ZF-ubiquitin complex were successively prepared at concentrations (ratio) of 1.45:0.15 mM (r = 9.7), 0.87:0.15 mM (r = 5.8), and 0.24:0.15 mM (r = 1.6).

NMR Spectroscopy—NMR experiments were carried out at 25 °C on a Varian Inova 600-MHz spectrometer equipped with a cryoprobe. ^{1}H-^{15}N heteronuclear single quantum correlation spectra were recorded with 200 (90 ms) and 1024 (122 ms) complex points (acquisition times) in ^{15}N and ^{1}H, respectively. Average (^{1}H, ^{15}N) chemical shift changes upon binding were calculated as $\Delta\delta_{av} = [(\Delta\delta_H)^2 + (\Delta\delta_N/5)^2]^{1/2}$. The binding affinity ($K_D$) was estimated by fitting the ZF titration data, assuming a simple complex formation model and using nonlinear regression. ^{15}N relaxation data (T_1, T_2, and {^{1}H}-^{15}N NOE) were acquired by standard methods (23).

Docking—The docking was performed with HADDOCK 1.3 (24), with initial coordinates of NEMO ZF and ubiquitin taken from their structure in free form (Protein Data Bank entries 2JVX and 1D3Z, respectively) and by using 16 ambiguous interaction restraints. The latter were defined on the basis of the NMR chemical shift mapping, surface accessibility data, and the homology with the pol η UBZ signature motif.

Binding Affinity—Tryptophan fluorescence measurements were recorded on a PTI QuantaMaster spectrofluorimeter (PTI, Lawrenceville, NJ) at 22 °C. The excitation wavelength was set to 295 nm to minimize the contribution of the tyrosyl group. The fluorescence emission at 352 nm was measured using 20 μM peptide and 20–500 μM ubiquitin. The observed fluorescence (F_{obs}) was corrected for dilution and for fluorescence from ubiquitin alone. Data for the ZF(W) peptide were fitted by nonlinear regression using the equation ($F_{obs} - F_0$) = ($F_{max} - F_0$) [L]/(K_D + [L]) to solve the maximum fluorescence (F_{max}) and the dissociation constant (K_D), given [L] (ligand concentration), F_0 (fluorescence in the absence of ligand), and F_{obs}. The K_D for ZF(W) mutant peptides was estimated using the F_{max} value obtained for ZF(W). For ZF peptide folding experiments, ZF peptide stocks, prepared in the presence or absence of $ZnCl_2$, were diluted to 20 μM in 50 mM Tris-HCl (pH 7.5). The emission spectra (305–415 nm) for these peptides were recorded, the buffer contribution was subtracted, and the fluorescence quantum yields were determined using *N*-acetyl tryptophanamide (Sigma) as standard as described previously (25).

Plasmid Construction—A pcDNA3 vector encoding FLAG-tagged human NEMO protein (residues 2–419) was used to generate five NEMO mutant constructs, including point mutants M407V, Q411R, V414S, and M415S and a NEMO ZF deletion (ΔZF). Substitutions were chosen conservatively, so as not to perturb the overall structure of the ZF domain. The point mutations were generated using overlap PCR. The primer sequences used for PCR are available upon request. The final PCR product was digested with EcoRI and XhoI and ligated into the pcDNA3-FLAG vector. A NEMO construct lacking 25 C-terminal residues (ΔZF) was generated using PCR introducing a stop codon after residue 394. The PCR product was digested and cloned as described above.

Functional Complementation Experiments— 4 × 10^6 NEMO$^{-/-}$ Jurkat T cells (JM4.5.2) (26) were transfected with 3 μg of pcDNA3-FLAG (empty or with various NEMO constructs), 1 μg of Igκ-luciferase, and 300 ng of β-galactosidase plasmids using DEAE-dextran as described previously (27). After 24 h, cells were treated with TNF-α (10 ng/ml) for 4 h and then harvested. Luciferase activity in soluble cell extracts was measured as described (27). β-galactosidase activity was measured using the luminescent β-galactosidase detection kit (Clontech) according to manufacturer's instructions. The level of luciferase, representing NF-κB activity, was normalized to the level of β-galactosidase, representing transfection efficiency.

Immunoprecipitation and Western Blot Analysis—293T cells, grown in 6-well dishes, were transfected with 8 μl of Lipofectamine 2000 (Invitrogen) and 3 μg of pcDNA-FLAG plasmid (empty or with various NEMO constructs) and harvested 24 h after transfection. Cells were lysed in 25 mM Tris-phosphate (pH 7.8), 1 mM dithioerythritol, 1% Triton X-100, and 10% glycerol (for Western blot analysis) or in 50 mM Tris-HCl (pH 7.4), 150 mM NaCl, and 1% Triton X-100 (for immunoprecipitation). FLAG-NEMO was immunoprecipitated using the FLAG immunoprecipitation kit (Sigma) according to the manufacturer's protocol. FLAG-NEMO proteins were detected using anti-FLAG M2 (Sigma) or anti-NEMO (antibody B24, homemade)

antibodies, and ubiquitin was detected using anti-ubiquitin (antibody 6C1, Sigma) antibody.

RESULTS AND DISCUSSION

NEMO ZF Binds Ubiquitin—The binding of a NEMO ZF synthetic peptide (see the sequence in supplemental Fig. S1) to ubiquitin was probed by NMR chemical shift perturbation experiments. The ^1H and ^{15}N chemical shifts of several ubiquitin residues vary gradually from the free (Fig. 2A, *black*) to the bound state (*red*) upon the addition of ZF, as typically observed for a complex in fast exchange on the NMR time scale. Significant average chemical shift changes ($\Delta\delta_{av}$) or attenuations of peak intensities are observed for a number of residues (Fig. 2B), thus identifying the binding surface on ubiquitin. Most of these residues are spatially located around Leu-8, Ile-44, and Val-70, *i.e.* on the conserved hydrophobic region of the five-stranded β-sheet of ubiquitin typically recognized by UBDs (28) (see Fig. 4C). Backbone dynamics from ^{15}N relaxation measurements (T_1, T_2, and {^1H}-^{15}N NOE) were evaluated for the free and ZF-bound state of ubiquitin (Fig. 2C). Isotropic rotational correlation times, estimated from the T_1/T_2 ratios of nonflexible residues, are 4.3 and 6.3 ns for the free and bound ubiquitin, respectively. Despite the small difference, these values are in good agreement with theoretical values of ~4.1 and ~5.7 ns expected for globular molecules with respective molecular masses of 8.5 and 11.8 kDa, suggesting the formation of a 1:1 complex. Overall, the internal mobility of ubiquitin is not significantly affected by peptide binding, with rather uniform and unchanged T_1, T_2, and {^1H}-^{15}N NOE profiles. This denotes the formation of a stable complex, although slightly more conformational exchange can be detected on the microsecond to millisecond time scale, especially for residues Phe-4, Thr-7, Ile-13, Thr-14, Gln-41, Arg-42, Lys-48, Gln-49, His-68, Val-70, Leu-71, and Arg-72 in the five-stranded β-sheet, as seen from their relatively lower T_2 values in the bound state.

The binding affinity (K_D) of the ZF-ubiquitin complex was estimated to be ~280 ± 90 μM by NMR. Because we observed the presence of peptide aggregates at high ZF concentration (21), we confirmed this affinity by tryptophan fluorescence spectroscopy, using a synthetic peptide containing the F395W substitution, denoted as ZF(W) (see the sequence in supplemental Fig. S1). This substitution does not affect the ability of ZF(W) to properly fold upon the addition of zinc (Fig. 3B). As seen in Fig. 3A, an increase in fluorescence signal is observed during ubiquitin titration (*filled circles*), corresponding to a K_D of 253 ± 15 μM, which is within the range reported for other UBDs (10–500 μM) (28). Note that the K_D value from fluorescence data is in agreement with the one estimated by NMR, indicating that the F395W substitution does not markedly affect the interaction. Ubiquitin containing the I44A mutation does not bind ZF(W) (*filled triangle*), showing that the increase in fluorescence is due to the formation of a specific NEMO ZF-ubiquitin complex and that residue Ile-44 is crucial for binding to NEMO ZF.

Structural Model of the NEMO ZF-Ubiquitin Complex—In the ββα structure of NEMO ZF, a large hydrophobic cluster encompassing the hydrophobic side of the α-helix was anticipated to be a potential protein-binding surface (21). As seen on
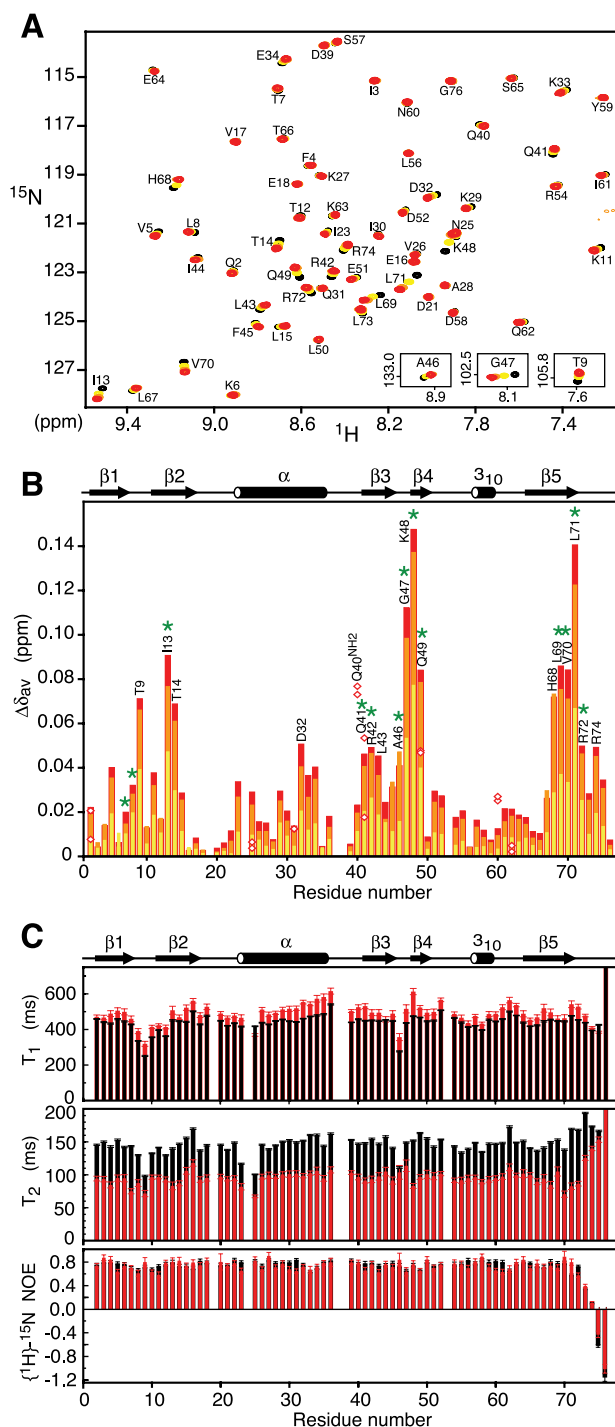

FIGURE 2. **NMR chemical shift perturbations of ubiquitin upon binding to NEMO ZF.** *A*, regions of ^1H-^{15}N heteronuclear single quantum correlation spectra obtained from the titration of 0.15 mM ^{15}N-labeled ubiquitin with increasing amounts of unlabeled ZF peptide (pH 6.2, 25 °C). ZF to ubiquitin ratios (*r*) were 0 (free ubiquitin, *black*), 1.6 (*yellow*), 5.8 (*orange*), and 9.7 (bound ubiquitin, *red*). *B*, weighted average chemical shift changes $\Delta\delta_{av}$ *versus* ubiquitin residue number for each *r* > 0 as defined in *A*, relative to *r* = 0. Values of $\Delta\delta_{av}$ are shown for the Asn and Gln side chain NH$_2$ groups (*red diamonds*) for *r* = 9.7. The *green asterisks* denote residues for which the relative peak intensities in bound ubiquitin are attenuated as compared with free ubiquitin. *C*, backbone dynamics of ubiquitin in its free form (*black*) and in complex with NEMO ZF (*red*, ZF-ubiquitin ratio of 9.7) from ^{15}N relaxation data. ^{15}N longitudinal (T_1) and transversal (T_2) relaxation times and {^1H}-^{15}N NOE values are plotted in the *top*, *middle*, and *bottom panel*, respectively. Secondary structure elements are indicated at the *top*.
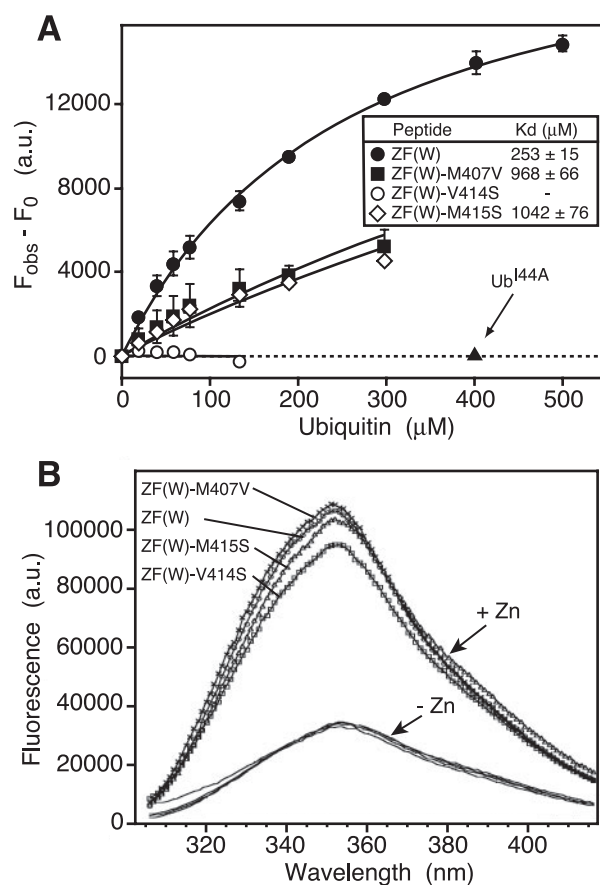
A

Peptide	Kd (μM)
ZF(W)	253 ± 15
ZF(W)-M407V	968 ± 66
ZF(W)-V414S	-
ZF(W)-M415S	1042 ± 76

B

FIGURE 3. **Ubiquitin binding affinities and folding of NEMO ZF peptides assayed by tryptophan fluorescence.** *A*, the change of fluorescence emission ($F_{obs} - F_0$) upon ubiquitin titration is shown for ZF(W) and three ZF(W) mutants (see *inset*). Titrations were performed with 20 μM peptide. *Error bars* represent standard deviations from two independent experiments. The dissociation constants (K_D) are given in the *inset*. No binding was observed in the presence of ZF(W) peptide and the ubiquitin I44A mutant (Ub^{I44A}, *filled triangle*). *a.u.*, absorbance units. *B*, ZF(W) mutant peptides fold similarly upon the addition of zinc. The emission spectra (305–415 nm), subtracted from buffer alone, were obtained upon tryptophan excitation at 295 nm. ZF(W) peptides at 20 μM were assayed in the absence (−*Zn*) or presence (+*Zn*) of zinc. The addition of zinc leads to a similar increase in fluorescence for all ZF(W) peptides, indicating that the mutations do not disrupt global zinc finger folding.

Fig. 4*A*, this region shares similarities with other ubiquitin-binding helices, notably with that of the pol η UBZ domain (22) and, to a lesser extent, with the inverted ubiquitin-interacting motif (UIM) of Rabex-5 (29, 30). Key residues at positions −7, −4, −3, −1, and +3 that are important for binding are conserved in NEMO ZF, whereas the central invariant Ala (position 0) is replaced by a Met. The binding interfaces on NEMO ZF (Fig. 4*B*) and on ubiquitin (Fig. 4*C*) were therefore defined according to the sequence homology with the UBZ motif and to the NMR chemical shift perturbation data, respectively.

On the basis of these two interfaces, we determined a docking model of the ZF-ubiquitin complex (Fig. 4*D*), using the HAD-DOCK program (24). We found that the hydrophobic side of the ZF α-helix interacts with the typically recognized hydrophobic region around Ile-44 of ubiquitin in a similar manner as the UBZ α-helix (see Fig. 3*D* of Ref. 22). Differences are, however, evident in the overall binding mode of the zinc fingers. Notably, the 4-residue shift observed from the relative position of the last 2 zinc-chelating residues in the sequence alignment

translates into a shift of the NEMO helix by more than one turn into the ubiquitin C terminus direction and leads to a slightly different orientation of the finger with respect to ubiquitin. These differences are in agreement with the fact that the α-helix in NEMO ZF is shorter than in the pol η UBZ by about one helical turn. The interaction between ubiquitin and NEMO ZF leads to a buried surface area of 1014 ± 55 Å² and is largely driven by hydrophobic forces, involving all or part of the side chains of Gln-411, Ile-412, Val-414, Met-415, and Ile-418 of the ZF and notably the ubiquitin residues Leu-8, Ile-44, and Val-70. In the pol η UBZ, the mutation of the central invariant Ala into a Phe was shown to abolish binding. However, in NEMO ZF, the residue Met-415 at the equivalent position inserts perfectly into the hydrophobic cleft formed by Leu-8, Ile-44, His-68, and Val-70, suggesting local differences between the pol η UBZ and the NEMO ZF around this position. In addition to these numerous hydrophobic contacts, the side chains of Asp-408 and Gln-411 at positions −7 and −4, respectively, likely contribute to the binding by allowing the formation of hydrogen bonds with the backbone amide or carbonyl groups of the loop residues Ala-46 to Lys-48 of ubiquitin, in a similar way as the corresponding Glu and Asp residues in the pol η UBZ.

To validate our model of the NEMO ZF-ubiquitin complex, we examined the ability of three modified ZF(W) peptides to interact with ubiquitin using fluorescence. In addition to the F395W substitution, these ZF(W) peptides contain the point mutation M407V (identified in a patient with the incontinentia pigmenti pathology (31)), V414S, or M415S. The ZF(W)-M407V and ZF(W)-M415S peptides show an ~4-fold decrease in binding affinity, and ZF(W)-V414S displays the greatest defect, with a complete loss in ubiquitin binding (Fig. 3*A*). Note that the fluorescence quantum yields in the presence of zinc are similar for all peptides, indicating that the reduced binding affinity of these peptides is not due to a global perturbation of the NEMO ZF fold (Fig. 3*B* and supplemental Table S1). These mutagenesis results are fully consistent with our model, attesting that residues Val-414 and Met-415, which lay on the central hydrophobic part of the interface, are crucial for ubiquitin binding. Furthermore, the reduced binding affinity observed for the pathogenic M407V mutant likely results from the loss of peripheral hydrophobic contacts between the long Met-407 side chain and Lys-48 (Fig. 4*D*).

Biological Relevance of the NEMO ZF-Ubiquitin Interaction in Vivo—Next, we addressed the question whether the interaction between NEMO ZF and ubiquitin is important for NF-κB activation. Using the full-length protein, we investigated whether ZF mutations located at the binding interface (M407V, Q411R, V414S, and M415S) are able to restore NF-κB activation in NEMO-deficient T-lymphocytes using an NF-κB-inducible luciferase reporter assay. Transfection of NEMO-expressing plasmids does not lead to a significant increase in luciferase activity in the absence of TNF-α (data not shown). On the other hand, stimulation with TNF-α leads to a 60-fold increase in activity in NEMO WT-expressing cells (set at 100%) as compared with empty plasmid (mock) control (Fig. 5*A*). All NEMO mutant constructs display a defect in NF-κB signaling to varying extents, M407V being the least severe (50% activity as compared with WT). Most notably, NEMO point mutations
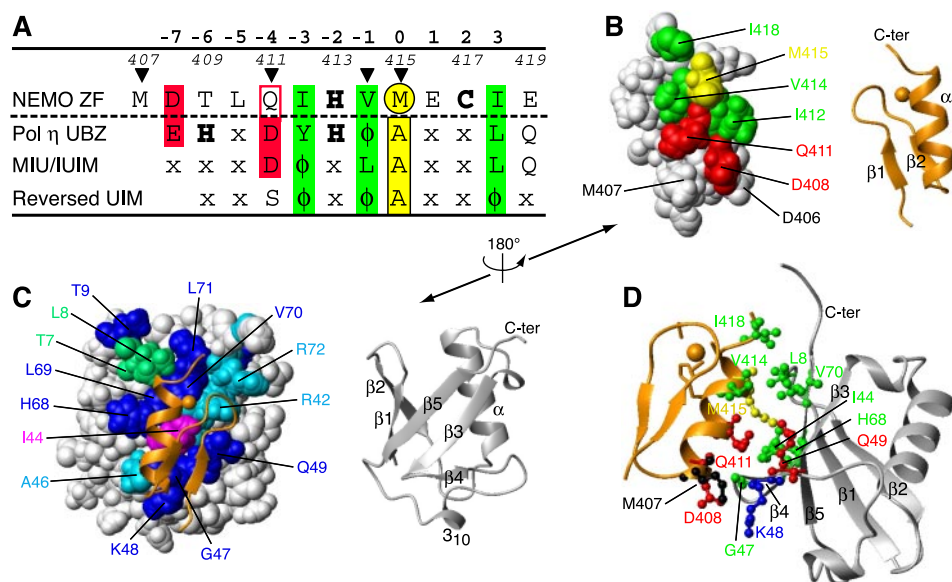
FIGURE 4. **Model of the NEMO ZF-ubiquitin complex.** *A*, alignment of the NEMO ZF sequence with the signature motifs of pol η UBZ, inverted UIM (*MIU/IUIM*), and reversed UIM. Human NEMO numbering is indicated in *italics*. The central invariant Ala in *yellow* (referred to as position 0) is replaced by a Met in NEMO ZF. Conserved hydrophobic residues are in *green*, and acidic residues are in *red*. φ and *X* denote large hydrophobic and "any" residues, respectively. Zinc ligands are in *bold*. NEMO mutations assessed in this study are indicated by *triangles* (M407V, Q411R, V414S, and M415S). *B*, spacefill and ribbon representations of NEMO ZF with the ubiquitin-binding surface color-coded as in *A*. *C-ter*, C-terminus. *C*, spacefill and ribbon representations of ubiquitin showing the ZF-binding surface as identified by the NMR chemical shift perturbations: $\Delta\delta_{av} > 0.041$ ppm in *light blue* and $\Delta\delta_{av} > 0.06$ ppm in *dark blue*. Residues with no perturbation but attenuated peak intensities in the bound form are in *green* (Fig. 2*B*). Ile-44 is colored in *magenta*. NEMO ZF in our docking model is shown in *orange*. *D*, docking model proposed for the NEMO ZF-ubiquitin complex (average structure), with the ZF in *orange* and ubiquitin in *gray*. The interface residues are shown as *balls* and *sticks* (*green*, *red*, and *blue* correspond to hydrophobic, acidic, and basic residues, respectively, and *yellow* is for the ZF central Met). The buried surface area is 1014 ± 55 Å².

proteins are detected at similar levels upon transfection (Fig. 5*B*). Therefore, mutations of ZF residues that exhibit a defect in ubiquitin binding impair TNF-α-induced NF-κB signaling in T lymphocytes, highlighting the importance of ubiquitin recognition by the ZF motif, mostly via crucial hydrophobic contacts.

We finally examined whether the M415S mutation, which shows the most severe defect in NF-κB signaling, affects the ability of NEMO to bind ubiquitinated proteins *in vivo*. Pull-down of FLAG-tagged NEMO WT protein after transient transfection in 293T cells leads to co-elution of a pattern of ubiquitinated proteins, whereas less ubiquitinated proteins co-elute with NEMO M415S (Fig. 5*C*). Hence, such a mutation in the ubiquitin-binding surface of the ZF reduces the ability of NEMO to bind ubiquitinated proteins, indicating that NEMO ZF is involved in ubiquitin binding *in vivo*.

Altogether, our results clearly reveal the role of the ZF as a novel ubiquitin-binding domain in NEMO, namely of the UBZ type, thereby providing new insights into the mechanism of ubiquitin recognition by NEMO to activate the NF-κB pathway. The moderate ZF affinity for ubiquitin, allowing transient complex formation, might be increased in the context of the full-length protein, which contains another UBD in the CC2-LZ domain. We propose that the ZF acts in a cooperative manner with the CC2-LZ domain to strengthen ubiquitin recognition and to preferentially bind polyubiquitin chains rather than monoubiquitin. Finally, our results suggest that, like other ectodermal dysplasia with immunodeficiency and incontinentia pigmenti mutations located in the CC2-LZ UBD, pathological mutations in NEMO ZF likely impair NF-κB activation by disrupting the binding to ubiquitin.
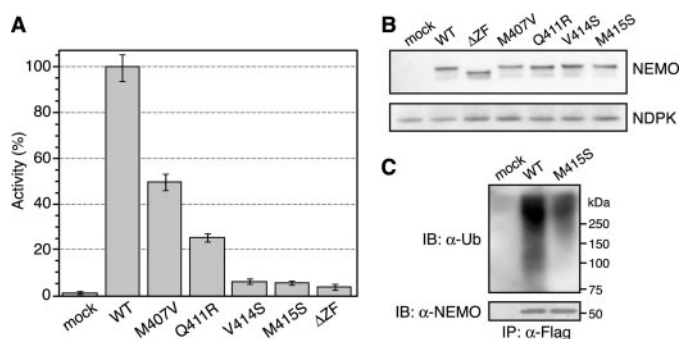
FIGURE 5. **In vivo analysis of mutations in the NEMO ZF UBD.** *A*, mutations in NEMO ZF result in a defect in TNF-α-induced NF-κB activation. NEMO-deficient Jurkat cells were co-transfected with an NF-κB-inducible luciferase reporter plasmid and an empty plasmid (*mock*) or a plasmid expressing FLAG-tagged NEMO: WT, point mutants M407V, Q411R, V414S, or M415S, or ZF-deleted (ΔZF). Cells were stimulated with TNF-α, and luciferase activity was measured after 4 h. Data represent two independent experiments performed in duplicate. *B*, NEMO WT and mutant constructs are expressed at similar levels. FLAG-NEMO proteins were detected upon transfection in 293T cells by immunoblot using anti-FLAG antibody (nucleoside diphosphate kinase (*NDPK*) is shown as an internal control). *C*, a mutation in NEMO ZF leads to a defect in ubiquitin binding *in vivo*. Lysates from 293T cells transfected with mock plasmid or plasmid encoding FLAG-NEMO WT or M415S were immunoprecipitated (*IP*) with anti-FLAG antibody. Immunoprecipitates were analyzed by immunoblot (*IB*) using anti-ubiquitin (α-*Ub*, *top panel*) or anti-NEMO (α-*NEMO, bottom panel*) antibody.

V414S and M415S are just as inefficient in activating NF-κB as the ΔZF construct (~5% residual activity). The inability to stimulate NF-κB signaling in these cells is not due to altered NEMO protein expression or solubility because all NEMO

REFERENCES
1. Hayden, M. S., and Ghosh, S. (2004) *Genes Dev.* **18,** 2195–2224
2. Fontan, E., Traincard, F., Levy, S. G., Yamaoka, S., Veron, M., and Agou, F. (2007) *FEBS J.* **274,** 2540–2551
3. Miller, B. S., and Zandi, E. (2001) *J. Biol. Chem.* **276,** 36320–36326
4. Hacker, H., and Karin, M. (2006) *Science's STKE* **2006,** re13
5. Sebban, H., Yamaoka, S., and Courtois, G. (2006) *Trends Cell Biol.* **16,** 569–577

6. Agou, F., Traincard, F., Vinolo, E., Courtois, G., Yamaoka, S., Israel, A., and Veron, M. (2004) *J. Biol. Chem.* **279,** 27861–27869
7. Tegethoff, S., Behlke, J., and Scheidereit, C. (2003) *Mol. Cell. Biol.* **23,** 2029–2041
8. Ea, C. K., Deng, L., Xia, Z. P., Pineda, G., and Chen, Z. J. (2006) *Mol. Cell* **22,** 245–257
9. Wu, C. J., Conze, D. B., Li, T., Srinivasula, S. M., and Ashwell, J. D. (2006) *Nat. Cell Biol.* **8,** 398–406
10. Zhou, H., Wertz, I., O'Rourke, K., Ultsch, M., Seshagiri, S., Eby, M., Xiao, W., and Dixit, V. M. (2004) *Nature* **427,** 167–171
11. Abbott, D. W., Wilkins, A., Asara, J. M., and Cantley, L. C. (2004) *Curr. Biol.* **14,** 2217–2227
12. Huang, T. T., Wuerzberger-Davis, S. M., Wu, Z. H., and Miyamoto, S. (2003) *Cell* **115,** 565–576
13. Tang, E. D., Wang, C. Y., Xiong, Y., and Guan, K. L. (2003) *J. Biol. Chem.* **278,** 37297–37305
14. Temmerman, S. T., Ma, C. A., Borges, L., Kubin, M., Liu, S., Derry, J. M., and Jain, A. (2006) *Blood* **108,** 2324–2331
15. Yang, F., Yamashita, J., Tang, E., Wang, H. L., Guan, K., and Wang, C. Y. (2004) *J. Immunol.* **172,** 2446–2452
16. Huang, T. T., Feinberg, S. L., Suryanarayanan, S., and Miyamoto, S. (2002) *Mol. Cell. Biol.* **22,** 5813–5825
17. Makris, C., Roberts, J. L., and Karin, M. (2002) *Mol. Cell. Biol.* **22,** 6573–6581
18. Wu, Z. H., and Miyamoto, S. (2007) *J. Mol. Med.* **85,** 1187–1202
19. Fusco, F., Pescatore, A., Bal, E., Ghoul, A., Paciolla, M., Lioi, M. B., D'Urso, M., Rabia, S. H., Bodemer, C., Bonnefont, J. P., Munnich, A., Miano, M. G., Smahi, A., and Ursini, M. V. (2008) *Hum. Mutat.* **29,** 595–604
20. Nenci, A., and Pasparakis, M. (2006) in *NF-κB: 20 Years on the Road from Biochemistry to Pathology* (A. Israël, D. Baltimore, and Y. M. Ben-Neriah, eds), Abstract 271, p. 84, Keystone Symposia, Banff, Canada
21. Cordier, F., Vinolo, E., Veron, M., Delepierre, M., and Agou, F. (2008) *J. Mol. Biol.* **377,** 1419–1432
22. Bomar, M. G., Pai, M. T., Tzeng, S. R., Li, S. S., and Zhou, P. (2007) *EMBO Rep.* **8,** 247–251
23. Kay, L. E., Nicholson, L. K., Delaglio, F., Bax, A., and Torchia, D. A. (1992) *J. Magn. Reson.* **97,** 359–375
24. Dominguez, C., Boelens, R., and Bonvin, A. M. (2003) *J. Am. Chem. Soc.* **125,** 1731–1737
25. Deville-Bonne, D., Sellam, O., Merola, F., Lascu, I., Desmadril, M., and Veron, M. (1996) *Biochemistry* **35,** 14643–14650
26. Harhaj, E. W., Good, L., Xiao, G., Uhlik, M., Cvijic, M. E., Rivera-Walsh, I., and Sun, S. C. (2000) *Oncogene* **19,** 1448–1456
27. Vinolo, E., Sebban, H., Chaffotte, A., Israel, A., Courtois, G., Veron, M., and Agou, F. (2006) *J. Biol. Chem.* **281,** 6334–6348
28. Hicke, L., Schubert, H. L., and Hill, C. P. (2005) *Nat. Rev. Mol. Cell Biol.* **6,** 610–621
29. Lee, S., Tsai, Y. C., Mattera, R., Smith, W. J., Kostelansky, M. S., Weissman, A. M., Bonifacino, J. S., and Hurley, J. H. (2006) *Nat. Struct. Mol. Biol.* **13,** 264–271
30. Penengo, L., Mapelli, M., Murachelli, A. G., Confalonieri, S., Magri, L., Musacchio, A., Di Fiore, P. P., Polo, S., and Schneider, T. R. (2006) *Cell* **124,** 1183–1195
31. Smahi, A., Courtois, G., Vabres, P., Yamaoka, S., Heuertz, S., Munnich, A., Israel, A., Heiss, N. S., Klauck, S. M., Kioschis, P., Wiemann, S., Poustka, A., Esposito, T., Bardaro, T., Gianfrancesco, F., Ciccodicola, A., D'Urso, M., Woffendin, H., Jakins, T., Donnai, D., Stewart, H., Kenwrick, S. J., Aradhya, S., Yamagata, T., Levy, M., Lewis, R. A., and Nelson, D. L. (2000) *Nature* **405,** 466–472

The Zinc Finger of NEMO Is a Functional Ubiquitin-binding Domain

Florence Cordier, Olivera Grubisha, François Traincard, Michel Véron, Muriel Delepierre and Fabrice Agou

Access the most updated version of this article at doi: 10.1074/jbc.M806655200

Alerts:
- When this article is cited
- When a correction for this article is posted

Click here to choose from all of JBC's e-mail alerts

Supplemental material:
http://www.jbc.org/content/suppl/2008/12/09/M806655200.DC1

This article cites 30 references, 11 of which can be accessed free at
http://www.jbc.org/content/284/5/2902.full.html#ref-list-1